ENGINEERING JOURNAL

Article

N-[3-(Trimethoxysilyl)propyl]ethylenediamine Functionalized Saponite as Adsorbent of Nickel from Aqueous Solution

Is Fatimah[a,*] **and Septian P. Yudha**[b]

Chemistry Department, Universitas Islam Indonesia, Kampus Terpadu UII, Jl. Kaliurang Km 14, Sleman Yogyakarta 55584, Indonesia
Email: [a]isfatimah@uii.ac.id (Corresponding author), [b]septian.yudha@gmail.com

Abstract. Surface modification of saponite clay by surface functionalization using N-[3-(Trimethoxysilyl)propyl]ethylenediamine was performed. This study of the physicochemical characteristics of modified saponite as a function of its functional compound content was investigated using XRD, a gas sorption analyzer, FTIR, TG analysis and SEM. It was observed that the content of N-[3-(Trimethoxysilyl)propyl]ethylenediamine increases the basal spacing (d001) of the saponite structure, which changes the specific surface area and surface profile of the solid. The study of nickel adsorption provides evidence of the increased adsorption capacity of the modified saponite. The adsorption follows pseudo-second order kinetics and fits the Langmuir, Temkin and Dubinin-Radushkevich (D-R) adsorption isotherms. Increased content of the modifying agent results in increased adsorption capacity. The material is reusable because regenerated materials retain greater than 90% of the adsorption capacity of fresh material.

Keywords: Saponite, N-[3-(Trimethoxysilyl)propyl]ethylenediamine, adsorption, intercalation.

ENGINEERING JOURNAL Volume 21 Issue 2
Received 11 July 2016
Accepted 4 October 2016
Published 31 March 2017
Online at http://www.engj.org/
DOI:10.4186/ej.2017.21.2.107

DOI:10.4186/ej.2017.21.2.107

1. Introduction

In addition to the advantages of industrial activities for economic growth, there are associated negative impacts on the environment. One of the byproducts of industrial activity is wastewater that requires treatment before its release to the environment. Therefore, further technological developments are needed not only to monitor these effluents but also to control them and improve wastewater treatment methods. Heavy metal contamination of wastewater has attracted significant attention, as demonstrated by the number of media reports focused it, and one of the heavy metals is nickel metal [1]. Nickel is usually used in industrial activities such as painting and leather production, as well as in the electrochemical and textile industries. Some adverse health impacts, including diarrhea, anemia, central nervous system are related to the presence of nickel in drinking water above the permissible limit of 0.02 mg/L (WHO drinking water quality standards). Therefore, it is important to reduce human exposure to nickel in drinking water. Several wastewater treatment methods, including electrochemical treatments, photoreduction, and other chemical treatments have been reported to decrease nickel content, but the adsorption technique is usually used in combination with these methods because the adsorption technique is usually used to reduce small amounts of metal content, to complement other methods [2]. Therefore, a selective, reusable and high-capacity nickel adsorbent is needed.

Many inorganic solids have been studied for nickel adsorption, including biosorbent, silica and modified silica, zeolite, modified carbon and clay minerals. Modification by surface functionalization of inorganic adsorbents was reported as a technique to enhance the adsorption capacity of these solids. For example, amine functionalized silica, MCM-41, and zeolite increase the adsorption capability of metal ions in aqueous solution [2–4]. As for clay minerals, modified sepiolite with [3-(2-aminoethylamino)propyl]trimethoxysilane was reported to have enhanced uptake of Ni(II), Cu(II), Mn(II), Zn(II), Fe(III) and Cd(II) ions from aqueous solutions. Similar mechanisms of metal adsorption, i.e., the formation of coordination bonding between heavy metal and N from the amine functional group of the modifying agent, play an important role in enhancing adsorption capacity. Among other inorganic materials, smectitic clay is a particularly useful adsorbent due to its high specific surface area and adsorption capacity. Due to the swellable capability of smectite structure, modification of the smectite interlayer with a relevant functional group to adsorb metals ion is a useful strategy. Due to its structure, smectite clay can be modified with organic compounds, such as quaternary ammine and aminosilane compounds. To build on some previously reported research related to the enhancement of adsorption capacity by attaching aminosilane compounds onto silica materials, the functionalization of smectite using aminosilane compounds was studied in this research. The enhancement of clay's adsorption capacity was reported for Pb(II) and chromate ion adsorption; the adsorption capacity was found to be greater than that of ammine functional groups in surfactant-modified montmorillonite and kaolinite [5–9]. Similar investigation reported not only adsorption capacity improvement but also that surfactant-modified clay also has reusable properties and can be used as a sustainable material for adsorption and pre-concentration purposes [10, 11].

Saponite was utilized as a model for smectite clay and N-[3-(Trimethoxysilyl)propyl]ethylenediamine, also known as ethylenediammine amino tetramethoxysilane (EDAPTMS) (its molecular structure is presented in Fig. 1), was chosen as the aminosilane compound for surface functionalization. A study of nickel adsorption by this material and the relationship between the adsorption and the material's physicochemical characteristics was the goal of this research. Certain chemical variables with complex interactions and environmental conditions could affect the mechanism and effectivity of metal adsorption by clay minerals. Additionally, the adsorption behavior of Ni in different pH conditions and the desorption capability are also presented.

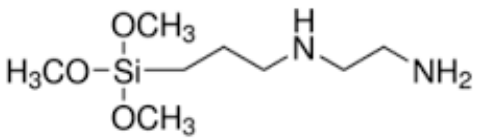

Fig. 1. Structure of EDAPTMS

2. Materials and Methods

2.1. Materials

Sumecton SA saponite mineral obtained from Kuninime Industry Co. Japan was used as received, and its chemical composition is listed in Table 1. Nickel sulfate pentahydrate and dimethyl sulfoxide(DMSO) and hydrochloric acid were purchased from Merck-Millipore while N-[3-(Trimethoxysilyl)propyl]ethylenediamine (EDAPTMS) was purchased from Sigma-Aldrich. Elemental analysis and cation exchange capacity as a related parameter of sumecton SA are listed in Table 1.

Table 1. Chemical composition of raw saponite.

Component	Content (%)	Analytical Method
Na_2O	3.75± 0.51	EDX-AAS
MgO	30.88± 0.51	EDX-AAS
Al_2O_3	6.39± 0.59	EDX-Gravimetri
SiO_2	58.97± 0.61	EDX-Gravimetri
FeO	--	AAS
CaO	--	AAS
Si/Al	7.83	
(Si+Al)/Mg	1.45	
CEC	99-102	Cu^{2+} adsorption -AAS

2.2. Methods

EDAPTMS-SAP was synthesized by first preparing a saponite suspension in DMSO-water (1:1) until the concentration of the suspension was 5%wt. The suspension was then stirred overnight at room temperature. EDAPTMS was then dispersed into the suspension, which was then refluxed for 4 h with the addition of 10 ml of 0.1 M HCl. The gel obtained was washed with water and then dried at 60°C ground to produce EDAPTMS-intercalated saponite (hereafter called EDAPTMS-SAP). The ratio of the molarity of EDAPTMS to the saponite weight was varied between 5 mmol/g and 15 mmol/g. The prepared materials were then characterized by x-ray diffraction (XRD) analysis, gas sorption analysis and Fourier-Transform Infra-Red spectrophotometry. An XRD Shimadzu X6000 instrument with Ni-filtered Cu Kα radiation was used for the XRD measurements. For the surface analysis, a NOVA 1200e Quantachrome instrument with N_2 gas adsorption under 77K was used and a Perkin Elmer FTIR was utilized for the analyses. SEM analysis was performed using a Phenom-X instrument and thermal gravimetric analysis (TGA) was conducted with a PT-1600 instrument.

For adsorption experiments, a batch adsorption system was utilized. Adsorbent powder was added into a nickel solution under stirring at 1000 rpm for various adsorption times. The solution was then filtered with Whatman filter paper. The filtrates were analyzed for Ni content using a Buck Scientific atomic absorption spectrometer. The Ni adsorbed with each treatment was calculated as the difference between the amount of Ni in the initial solution and that remaining after adsorption. For the adsorption kinetic simulation, Freundlich, Langmuir and Temkin adsorption model were simulated based on the varied nickel initial concentration.

3. Results and Discussion

3.1. Material Characterization

The preparation of EDAPTMS-SAP based on the EDAPTMS hydrolysis mechanism in acid condition shown in Fig. 2 refers to hydrolysis-condensation kinetics [12–14]:

DOI:10.4186/ej.2017.21.2.107

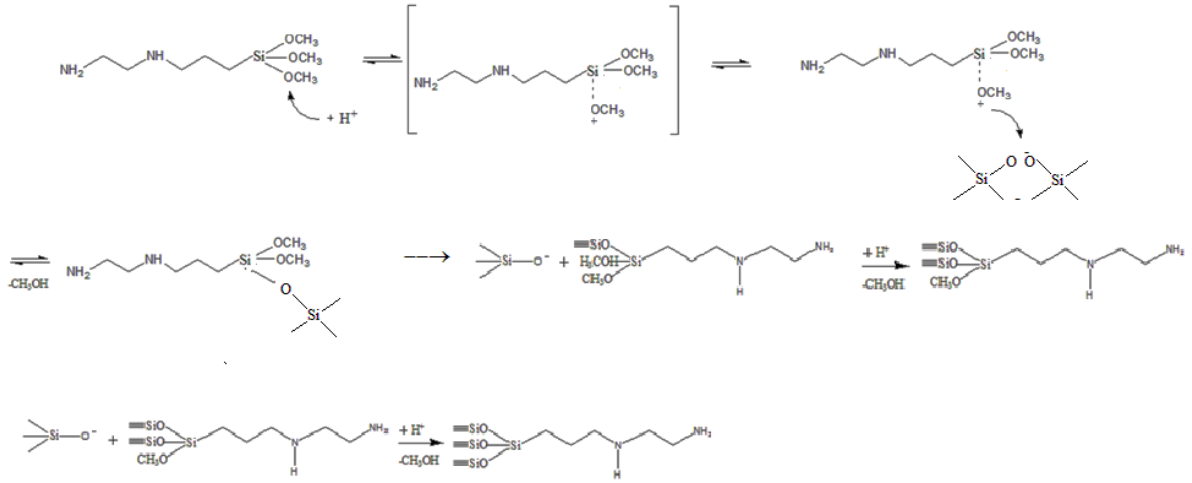

Fig. 2. Mechanism of saponite functionalization by EDAPTMS.

EDAPTMS is inserted via a sol-gel method by substituting $–OCH_3$ from EDAPTMS and bonding with –O-Si from a silica sheet with a saponite structure. Due to the presence of acid in the mixture demethanolization occurs and the interlayered structure of clay is anchored by alkylammine functional groups.

The physicochemical characteristics of EDAPTMS-SAP were analyzed by XRD in order to evaluate changes to the d_{001} basal spacing after the insertion of EDAPTMS. The reflections are presented in Fig. 3.

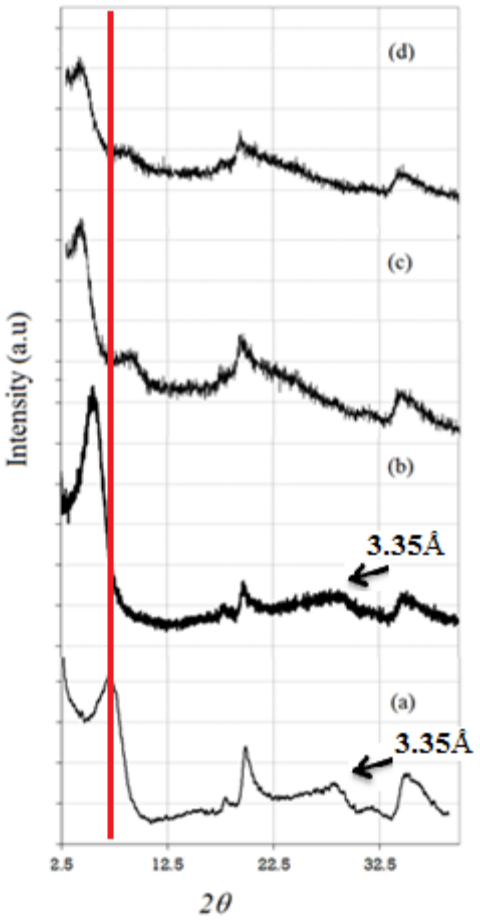

Fig. 3. XRD pattern of (a) SAP (b) EDAPTMS-SAP1 (c) EDAPTMS-SAP3 (d) EDAPTMS-SAP5.

This pattern shows that all samples represent the saponite mineral from specific reflections at 2θ= 6.08°; 19.84° and 35.08°, which correspond to d_{001}, d_{002} and d_{006} reflections at values of d_{001}=12.44 Å, d_{002}= 4.46 Å and d_{006}= 2.52 Å. The shifted d_{001} values were identified after EDAPTMS modification. Due to the variations depending on the EDAPTMS contents, it was concluded that there is significant change in the shifting reflection such that higher EDAPTMS content produced increased d_{001} basal spacing. EDAPTMS-SAP1 shows an increase of d001 to 17.94 Å as result of intercalated EDAPTMS in the interlayer space of the saponite. Broad reflections appeared from EDAPTMS-SAP3 and EDAPTMS-SAP5. The double reflections that correspond to 17.92 Å and 8.79 Å are found in EDAPTMS-SAP3, while these reflections are associated with the basal spacing of 19.51 Å and 10.37 Å from EDAPTMS-SAP5, respectively. The double reflections may be the result of the possible conformation of organic compounds intercalated in clay in which the possible conformations include paraffinic, bilayer or pseudotrimolecular [15]. A similar trend was reported for surfactant-intercalated montmorillonite with cetyl trimethyl ammonium bromide(CTAB) and benzyloctadecyldimethylammonium chloride when the value of the surfactant molar ratio to cation exchange capacity was greater than 1 [16–18]. Specific peak at around 28° correspond to 3.35Å found in SAP and EDASAP-1 correspond to the presence of elemental silica probably in the form of quartz in very small quantity is identified. This peak is disappeared along increasing EDAPTMS due to the insertion of the molecules. The similar pattern is also reported from the modification of kaolin [19]. The identified conformation is also in agreement with the surface parameter evaluated from the N_2 adsorption-desorption profile (Fig. 4) and the calculated parameter (Table 2).

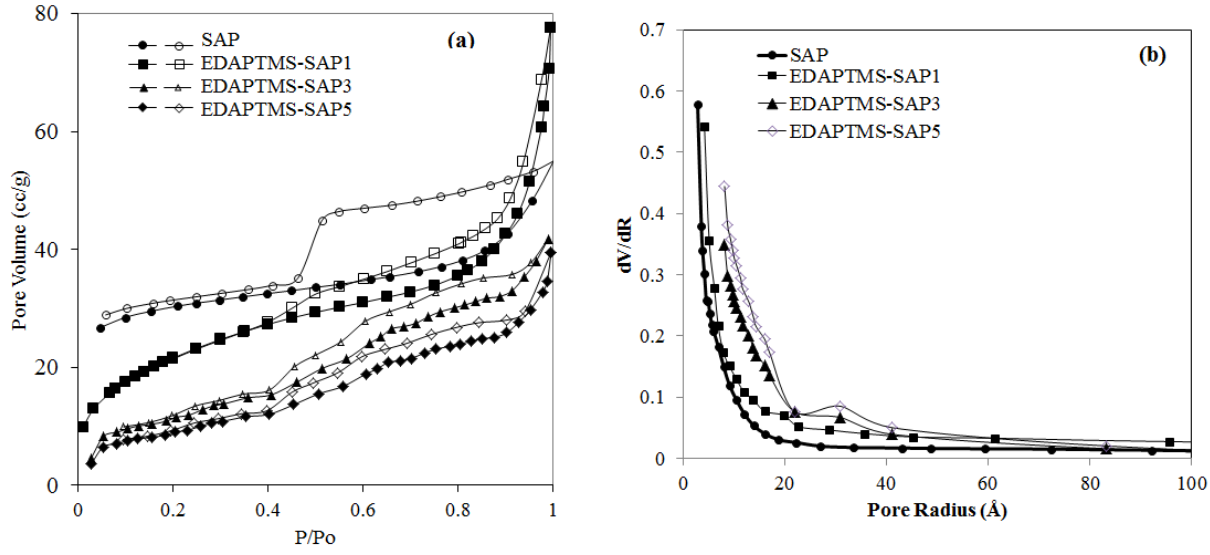

Fig. 4. (a) adsorption-desorption profile of materials; (b) Pore distribution of materials.

Table 2. Surface parameter of materials.

Sample	Specific surface area(m^2/g)	Pore Volume (cc/g)	Pore Radius (Å)
SAP	169.30	$21.34.10^{-2}$	14.58
EDAPTMS-SAP1	153.42	$15.78.10^{-2}$	14.50
EDAPTMS-SAP3	88.86	$9.32.10^{-2}$	13.24
EDAPTMS-SAP5	82.32	$7.65.10^{-2}$	9.89

The N_2 adsorption–desorption isotherms and the BJH desorption pore size distribution (Fig. 4) of EDAPTMS-SAPs demonstrate that all of the samples exhibit characteristic type IV isotherms and have a steep increase in adsorption at P/P0 = 0.6–0.8. Loops of this type are given by plate-like particles consisting of macropores that are not completely filled with pore condensate. The change in the adsorbed volume by saponite modification reflects the increasing specific surface area by EDAPTMS intercalation at a molar ratio to saponite's CEC of 1, but at higher ratios it is reduced since the increasing EDAPTMS

content results in the formation of other conformations, reducing the pore volume. When larger amounts of EDAPTMS are inserted into clay structures, lower specific surface areas are obtained. Additionally, the adsorption-desorption pattern exhibits the evolution of the hysterisis loop and multilayer adsorption represents mesoporous formation. This assumption is also validated by the pore distribution curve.

The change in surface character is also demonstrated by the SEM analysis results shown in Fig. 5. There is no significant change for EDAPTMS-SAP1 and EDAPTMS-SAP3 compared to SAP material, but EDAPTMS-SAP5 expresses a flaky and rougher surface that likely results from changes to the surface functionalization and surface profile evolution.

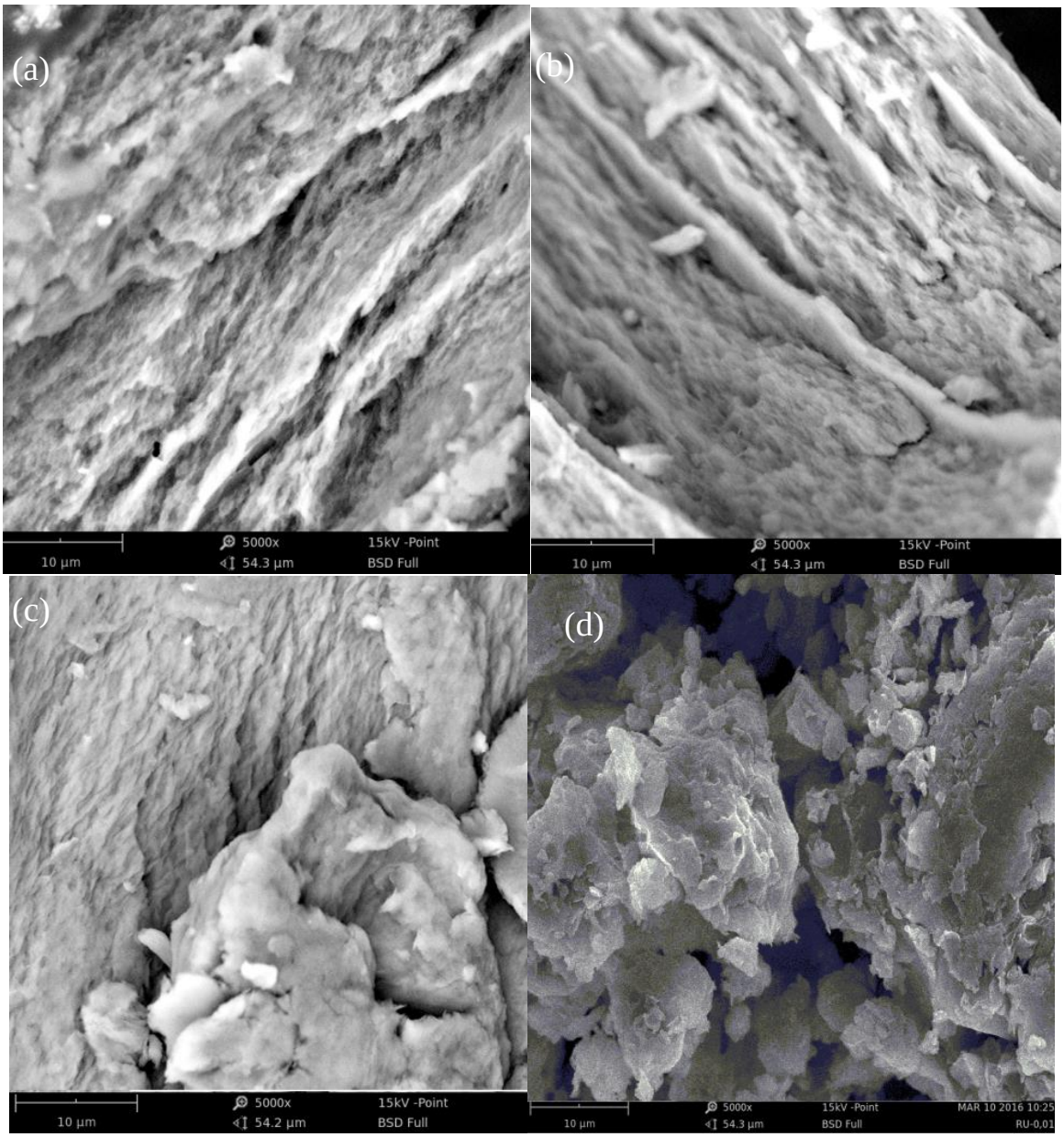

Fig. 5. SEM profile of (a) SAP; (b) EDAPTMS-SAP1; (c) EDAPTMS-SAP3; (d) EDAPTMS-SAP5.

The intercalated EDAPTMS is also represented by the thermal behavior of the initial clay and the intercalated clays, as shown in Fig. 6. The main changes revealed by thermal gravimetric analysis (TGA) of all sample are that temperatures of approximately 215 °C may be associated with the release of water absorbed in pores and also with the loss of ethylenediammine functional groups from EDAPTMS. By comparing the thermograms, and the weight loss in the region of 25-220°C, higher EDAPTMS contents reflect a higher mass reduction as temperature increases.

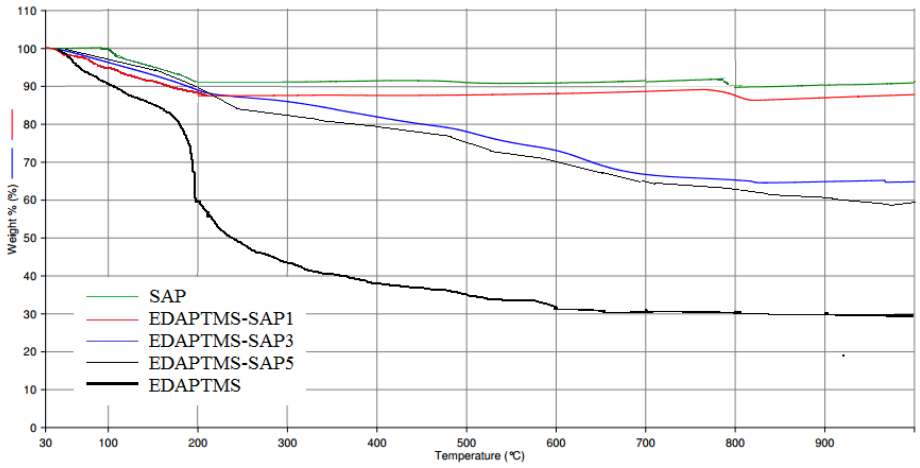

Fig. 6. TGA profile of the samples.

The presence of an amino functional group is identified by FTIR spectra in Fig. 7. There are some differences between the absorption rates of SAP and EDAPTMS-SAP. The peaks at 466.95 cm^{-1} and 1042.31 cm^{-1} are the specific vibration spectra of Si-O-Si from the clay structure. After modification with EDAPTMS there is a peak at 1388.97 cm^{-1} which indicates the presence of ($-CH_3$), and the peak at 2361.03 cm^{-1} is from stretching vibrations of aliphatic C-H and–CH_2-. The presence of N-H from EDAPTMS seems to overlap with –OH absorption from silanol (Si-OH) in the region of 3500-3100 cm^{-1}.

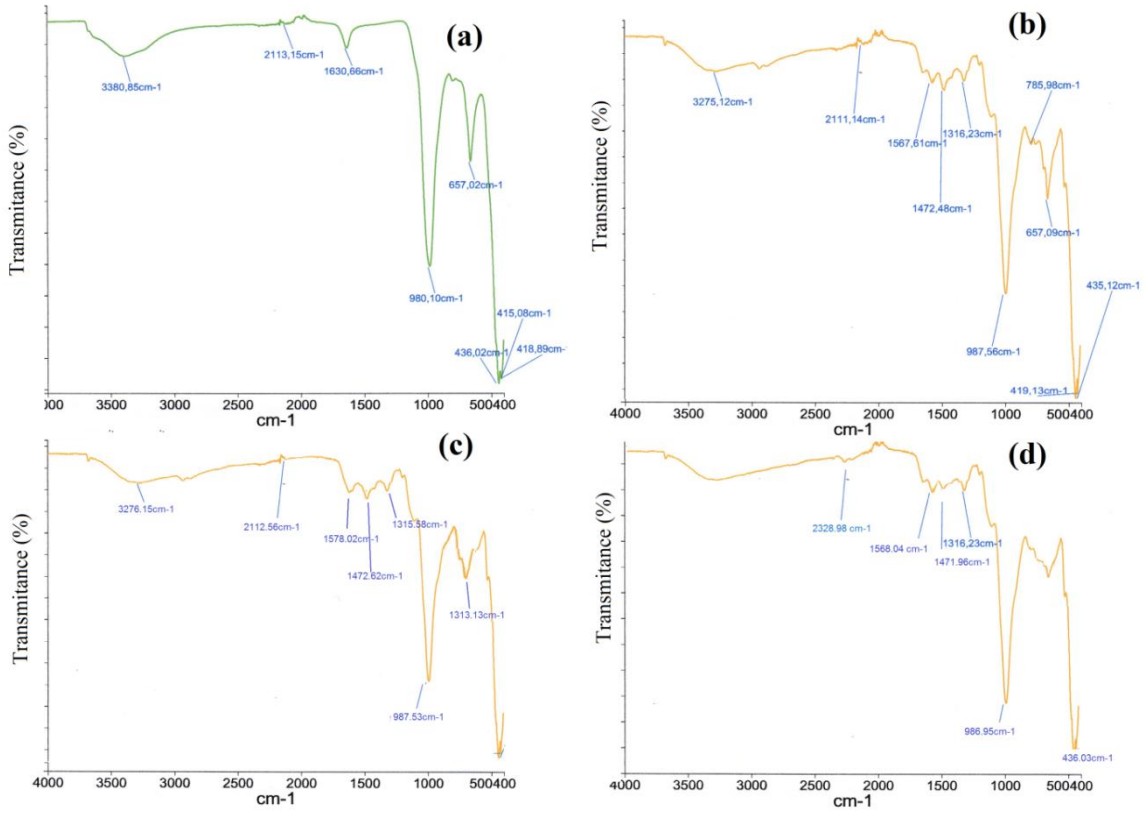

Fig. 7. FTIR spectra of (a) SAP (b) EDAPTMS-SAP1 (c) EDAPTMS-SAP3 (d) EDAPTMS-SAP5.

DOI:10.4186/ej.2017.21.2.107

3.2. Kinetic of Nickel Adsorption

The kinetics of nickel adsorption by EDAPTMS-SAPs and saponite samples is shown in Fig. 8.

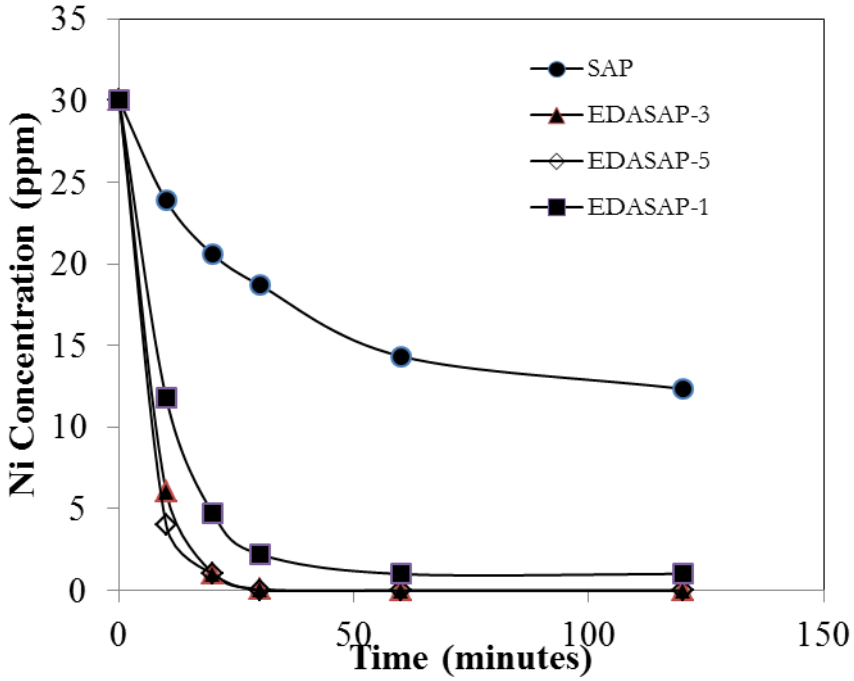

Fig. 8. Kinetics of nickel adsorption by materials (Initial concentration = 30 ppm; pH = 6.8).

Using the kinetics data from various initial concentrations, the mechanism of adsorption was investigated by using pseudo-first order, pseudo-second order, and Elovich models. The pseudo-first order model, also known as the Lagergern equation, is based on the assumption that the rate of adsorption site occupation is proportional to the number of unoccupied sites with the following equation:

$$\log(q_e - q_t) = \log q_e - (\frac{K_1 t}{2.303}) \quad (1)$$

where K_1 (min^{-1}) is the rate constant, and qt and qe are the amounts of metal ions adsorbed at time t and equilibrium, respectively. The pseudo-second order model is based on the assumption that the occupation of adsorption site is proportional to the square of the number of unoccupied sites with the following equation:

$$\frac{t}{q_t} = \frac{1}{K_2 q_e^2 + t/q_t} \quad (2)$$

with similar definitions of q_t and q_e as in pseudo first order equation.

Another kinetic model that is proposed is the Elovich model with the following equation:

$$q_t = \left(1/\beta\right) \ln(\alpha\beta) + \left(1/\beta\right) \ln t \quad (3)$$

where a is the initial adsorption rate of the Elovich equation (mg g^{-1} min^{-1}) and β is a constant related to the extent of surface coverage and activation energy for chemisorption. Both constants can be derived from the plot of q_t vs. ln$t$ *which* gives a slope of $(1/\beta)$ and an intercept of $1/\beta$ ln $(a\beta)$ as intercept.

The intra-particle diffusion model is linearly expressed as

$$q_t = k_{diff} t^{1/2} + C_{pi} \quad (4)$$

where k_{diff} is the intraparticle diffusion rate constant of stage i (mg g^{-1} $min^{-0.5}$) and is calculated by the slope of straight-line portion of the plot of q_t vs. $t^{1/2}$. C_{pi}, the intercept of stage *i*, is a representation of the thickness of boundary layer, indicating that the larger the intercept, the greater the boundary layer effect.

Calculated parameter data from three models is listed in Table 3.

Table 3. Calculation results of kinetics order simulation on nickel adsorption data by prepared materials.

Model	SAP	EDAPTMS-SAP 1	EDAPTMS-SAP 3	EDAPTMS-SAP 5
Pseudo first-order	K_1= 2.56.10^{-2} min^{-1} Qe = 36.69 mg/g R^2 = 0.9499	K_1= 13.94.10^{-1} min^{-1} Qe = 178.65 mg/g R^2 = 0.9817	K_1= 15.56.10^{-1} min^{-1} Qe = 179.20 mg/g R^2 = 0.9817	K_1= 24.21.10^{-1} min^{-1} Qe = 188.92 mg/g R^2 = 0.9415
Pseudo second-order	K_2= 43.68.10^{-2} min^{-1} Qe = 28.79 mg g^{-1} R^2 = 0.9995	K_2= 30.86.10^{-2} min^{-1} Qe = 44.74 mg/g R^2 = 0.9973	K_2= 31.97.10^{-2} min^{-1} Qe = 56.60 mg/g R^2 = 0.9987	K_2= 30.79.10^{-2} min^{-1} Qe = 75.84 mg/g R^2 = 0.9999
Elovich model	α= 87.95 mg $g^{-1}min^{-1}$ β = 21.52 mg.g^{-1} R^2= 0.8095	α= 33.29 mg $g^{-1}min^{-1}$ β = 30.03 mg.g^{-1} R^2= 0.4065	α= 33.05 mg $g^{-1}min^{-1}$ β = 30.25 mg.g^{-1} R^2= 0.2680	α= 5.56 mg $g^{-1}min^{-1}$ β = 179.59 mg.g^{-1} R^2= 0.2945
Intraparticle difussion	K_{diff}= 1.204 mg $g^{-1}min^{-0.5}$ C_{pi}= 4.078 R^2 = 0.9690	K_{diff}= 0.796 mg $g^{-1}min^{-0.5}$ C_{pi}= 20.438 R^2 = 0.6350	K_{diff}= 0.375 mg $g^{-1}min^{-0.5}$ C_{pi}= 25.981 R^2 = 0.3869	K_{diff}= 0.265 mg $g^{-1}min^{-0.5}$ C_{pi}= 27.195 R^2 = 0.5226

The calculated results demonstrate that the second-order kinetic model provides a good correlation for the adsorption of Ni^{2+} ions onto all adsorbents in contrast to the poorer fits of the pseudo-first-order, Elovich and intraparticle difussion models.

3.3. Adsorption Isotherm

Adsorption isotherms are usually applied to evaluate the experimental data of equilibrium adsorption. Based on the kinetics data, several isotherm models, including Langmuir and Freundlich, Temkin, Harkin-Jura and Dubinin-Radushkevich were used to acquire the best-fit isotherm and confirm the adsorption mechanism.

The isotherms are obtained by studying the relationship of the quantity of metal uptake per unit mass of sorbent to the equilibrium concentration of adsorbate in the bulk solution. Equation (5) indicates the general definition of the Langmuir isotherm:

$$q_e = q_m b \;\; C_e/(1 + b \;\; C_e) \tag{5}$$

as well as the linear form:

$$\frac{1}{q_e} = \left(\frac{1}{bQ_m}\right)\frac{1}{C_e} + \frac{1}{Q_m} \tag{6}$$

where q_e is the adsorbed content in equilibrium, C_e is the nickel concentration in equilibrium, and b and Q_m are the Langmuir adsorption constant and adsorption capacity in monolayer region, respectively. K_L is the energy constant related to the strength of sorption, and q_m is the maximum adsorption capacity of the solid phase.

The Freundlich model is generally expressed as

$$q_e = K_F C^{1/n} \tag{7}$$

and in the linear form:

$$lnq_e = lnK_F + \frac{1}{n_F} lnC_e \tag{8}$$

with similar definitions of qe and Ce as in Langmuir equation while K_F and $1/n_F$ are the Freundlich constants. Unlike the Langmuir equation, the Freundlich model cannot predict the sorption maximum. The maximum value of n is 1, at which K_F will be the same as the partitioning coefficient, which indicates the ratio of metal sorbed to that present in the batching solution at equilibrium.

For Temkin isotherm, following equation is applied:

$$q_e = \frac{RT}{b_T}\ln(K_T C_e) = B_T \ln(K_T C_e) \quad (9)$$

where $B_T = (RT)/b_T$, T is the absolute temperature in Kelvin and R is the universal gas constant (8.314 J/mol K). The model constants B_T and K_T are determined by the linear plot of q_e versus ln C_e. The Temkin isotherm assumes that the heat of adsorption of the molecules in a layer decreases linearly due to adsorbent–adsorbate interaction and that the binding energies are uniformly distributed.

Dubinin-Raduskevich:

$$lnq_e = lnQ_{DR} - K_{DR}\varepsilon^2 \quad (10)$$

with

$$\varepsilon = RTln\left(1 + \frac{1}{C_e}\right) \quad (11)$$

where (mmol g^{-1}) is the amount of metal ions adsorbed, Q_{DR} (mmol g^{-1}) is the maximum adsorption capacity of metal ions, K_{DR} (mol^2/kJ^2) is the Dubinin-Radushkevich isotherm constant, Ce (mol dm^{-3}) is the equilibrium concentration of metal ions, is the gas constant (8.314 J/mol K), and (K) is absolute temperature in Kelvin.

Table 4. Calculation results of adsorption isotherm by prepared materials.

Model	**SAP**	**EDAPTMS-SAP 1**	**EDAPTMS-SAP 3**	**EDAPTMS-SAP 5**
Langmuir				
Qm (mg/g)	19.277	135.164	142.661	148.532
KL	1.1366	2.6164	4.5557	1.4384
R^2	0.8941	0.9947	0.9798	0.9672
Freundlich				
KF(mmol g^{-1})(mol dm^{-3})$^{-1/n}$	3.977	41.322	58.038	58.440
n	1.160	2.893	2.146	4.013
R^2	0.8340	0.9544	0.7493	0.7028
Temkin				
BT	12.481	8.244	7.984	5.3899
KT	2.926	7.184	3.538	4.797
R^2	0.8583	0.9544	0.9710	0.9076
Dubinin-Raduskevich				
Q_{DR}(mg.g^{-1})	19.673	103.504	29.604	71.388
K_{DR}(kJoule^2/mg^2)	$2.31.10^{-7}$	9.111	$8.79.10^{-8}$	$8.21.10^{-8}$
E (KJoule)	1.968	19.039	21.602	24.580
R^2	0.9320	0.9991	0.9567	0.9405
Harkin-Jura				
A_{H-J}	7.022	13.999	14.299	15.882
B_{H-J}	-0.0068	-0.014	-0.0058	-0.0036
R^2	0.7896	0.9106	0.7260	0.9209

The Harkins-Jura isotherm model can be used to describe multilayer adsorption and the existence of heterogeneous pore distribution in the surface of adsorbents. This model can be expressed through the following Eq. (11):

$$\frac{1}{[q_e^2]} = \frac{[B_{HJ}]}{[A_{HJ}]} - \frac{1}{[A_{HJ}]}\log(C_e) \quad (11)$$

where B_{JH} and A_{HJ} are the Harkins-Jura constants. Both B_{HJ} and A_{HJ} can be determined from the slope and the intercept, respectively, of the linear plot based on $\frac{1}{[q_e^2]}$ versus $\log(C_e)$. The parameters of the adsorption simulation data are listed in Table 4.

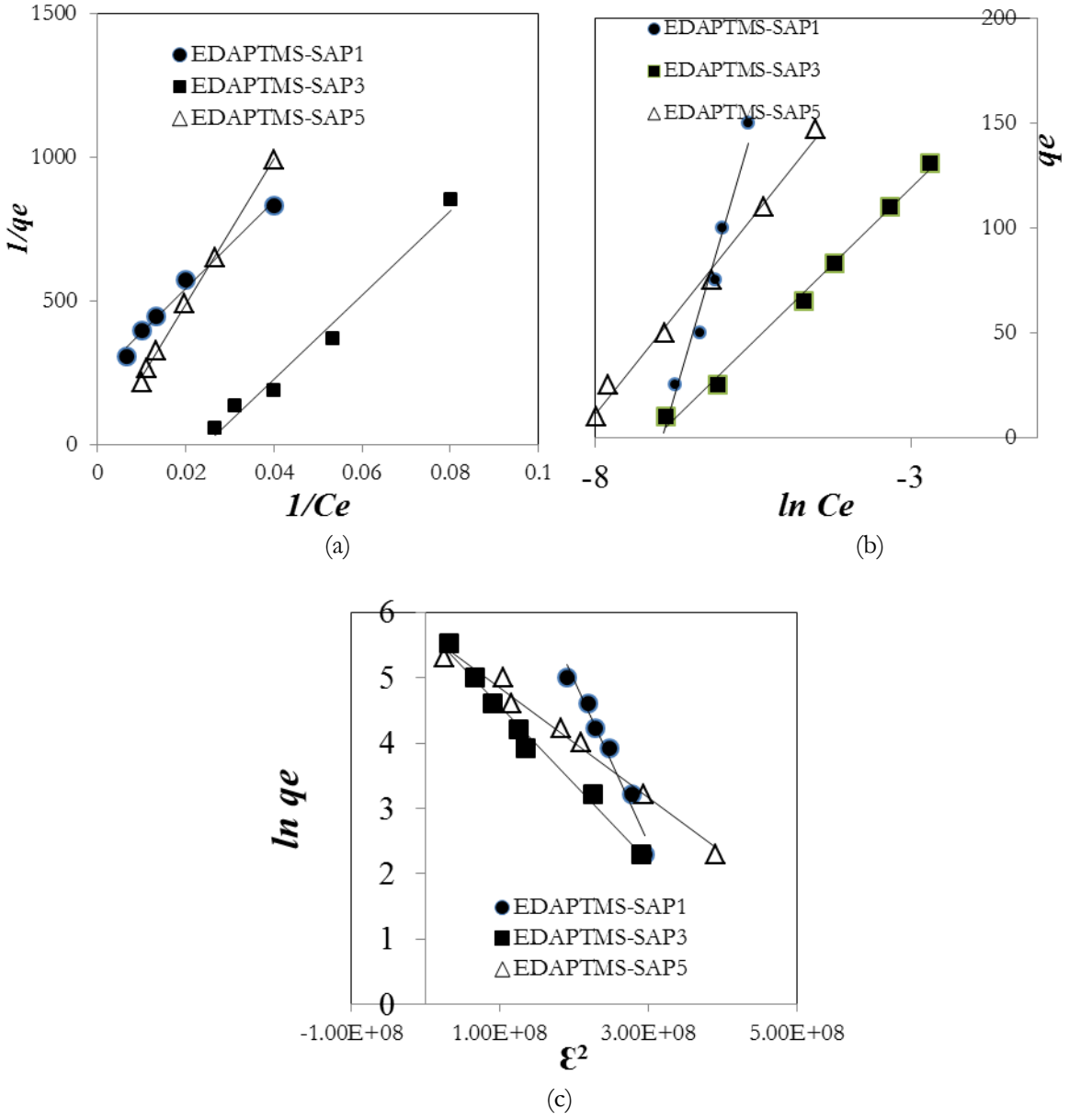

Fig. 9. Adsorption isotherm plot of (a) Langmuir model (b) Temkin model (c) D-R model.

The values of the determination coefficient (R^2) of the examined five isotherm models demonstrate that the Langmuir, Temkin and Dubinin-Radushkevich (D-R) isotherm models gave a significantly better fit than the other models for data from EDAPTMS-SAPs, as represented by the curve in Fig. 9. The coefficient of Freundlich and Harkin-Jura models was less than 0.9 except for EDAPTMS-SAP1. This result may be related to the mechanism that occurred during the adsorption process. The D-R model is related to adsorption with a Gaussian energy distribution onto a heterogeneous surface, and the model has often successfully fitted high solute activities and the intermediate range of concentrations data. The energy value can be used to distinguish the properties of metal adsorption. The adsorption mechanism can also be predicted from the values of E. When the E values are between 8 and 16 kJ/mol, the adsorption process proceeds by chemical adsorption, while if E < 8 kJ/mol, the adsorption process is a physically occurring process. The increasing E value associated with increasing EDAPTMS content suggests that the presence

of a functional group is linearly related to the increasing adsorption sites and confirms that nickel adsorption over EDAPTMS-SAPs is chemical adsorption.

The capacity of nickel adsorption by the materials in this work compared to those in other related investigations is listed in Table 5. Generally, the kinetics of nickel adsorption from aqueous solutions obey pseudo-second order kinetics and fit to Langmuir isotherm.

Table 5. Comparison on kinetics and adsorption isotherm of nickel adsorption by several adsorbent.

Adsorbent	Kinetics	Model	Adsorption capacity ($mg.g^{-1}$)	Reference
Natural Maghnite	Pseudo second order	Langmuir	18.95	[20]
Activated bentonite	Pseudo second order	Langmuir	19.6	[21]
Sepiolite functionalized with N-[3-(trimethoxysilyl)propyl]-ethylenediamine triacetic acid trisodium salt	Pseudo second order	Langmuir	7.308	[22]
Graphene oxide modified with 2,2'-dipyridylamine	Pseudo second order	Lagmuir	180.893	[23]
Nano-crystalline calcium hydroxyapatite	Pseudo second order	Langmuir	46.17	[24]
MCM-41/*N*-(3-trimethoxysilyl)-propyl)diethylenetriamine	Pseudo second order	Langmuir	58.47	[25]
amino functionalized MCM-41) and nano NH2-MCM-41	Pseudo first order	Langmuir	12.76	[3]
EDAPTMS-SAP1	Pseudo second order	Langmuir	135.164	This work
		Freundlich	41.322	
EDAPTMS-SAP3	Pseudo second order	Langmuir	142.661	This work
EDAPTMS-SAP5	Pseudo second order	Langmuir	148.532	This work

3.4. Effect of pH

The variation of the adsorption capability as a function of pH was evaluated at room temperature. Fig. 10 shows that the adsorption of nickel ions is optimized at pH = 7. The adsorption capacity of Ni(II) first increased as the pH increases, and after reaching pH=7 it became constant as pH increased. The strong electrostatic repulsion between the surface of the adsorbent and nickel accelerates the interaction of metal-electron pair donors from the N in EDAPTMS, but by increasing the pH, the repulsive ion-exchange mechanism is reduced. The change of the nickel hydroxide species in the solution may hinder the metal-binding process. This trend is quite similar to that associated with nickel adsorption by functionalized montmorillonite and soil [26, 27].

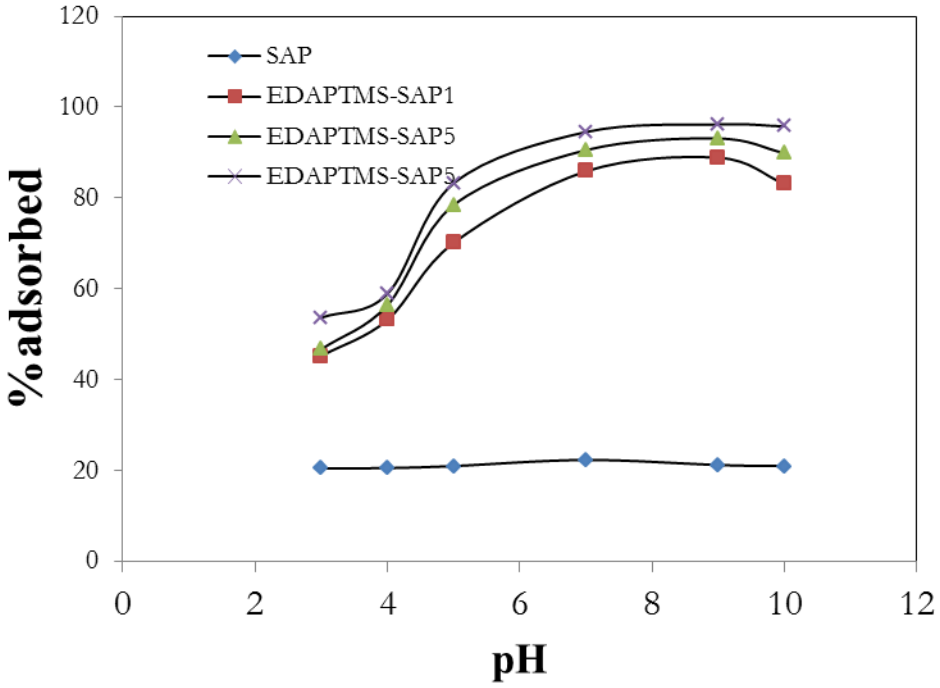

Fig. 10. Effect of pH on % nickel adsorption (Initial concentration of Nickel: 50 ppm, Time of adsorption: 2 hs).

3.5. Material Reusability

The ability to regenerate and reuse the adsorbent is an important property, because on an industrial scale, the reusability will allow for a more economical process. Adsorbent regeneration was performed by nickel leaching using 0.05 M HCl followed by heating at 100°C for 4 h. The percentage of desorbed nickel in the leaching is calculated by following Eq. (12):

$$Desorbed\ nickel\ (\%) = 100x\ \frac{Nickel\ content\ in\ leached\ solution}{Maximum\ nickel\ content\ in\ adsorbent} \quad (12)$$

The reusability data calculated by the percentage of adsorption capacity of reused adsorbent compared to fresh adsorbent are presented in Table 6.

Table 6. Desorbed nickel in adsorbent regeneration and its reusability.

Sample	Desorbed Nickel (%)	Reusability
SAP	90.23	95.87
EDAPTMS-SAP1	88.56	90.23
EDAPTMS-SAP3	87.65	90.25
EDAPTMS-SAP5	75.45	90.11

4. Conclusions

Functionalization of saponite with ethylene diamine amino propyl trimethoxisilane was successfully performed. The functional group on the saponite surface increases the specific surface area, pore volume and pore radius of the saponite as a reflection of the intercalation scheme as a function of EDAPTMS content. The results indicate that this functionalization enhances the nickel adsorption of saponite. Nickel adsorption obeys pseudo-second order adsorption kinetics and fits to Langmuir, Temkin and Dubinin-Radushkevich adsorption isotherms. The ability to regenerate and reuse this material is demonstrated, further indicating that this material is a promising adsorbent for the adsorption of nickel from water.

References

[1] M. W. Amer, F. I. Khalili, and A. M. Awwad, "Adsorption of lead , zinc and cadmium ions on polyphosphate-modified kaolinite clay," *Environmental Chemistry*, vol. 2, pp. 001–008, 2010

[2] J. Aguado, J. M. Arsuaga, A. Arencibia, M. Lindo, and V. Gascón, "Aqueous heavy metals removal by adsorption on amine-functionalized mesoporous silica," *Journal of Hazardous Materials*, vol. 163, pp. 213–221, 2009. doi:10.1016/j.jhazmat.2008.06.080.

[3] A. Heidari, H. Younesi, and Z. Mehraban, "Removal of Ni(II), Cd(II), and Pb(II) from a ternary aqueous solution by amino functionalized mesoporous and nano mesoporous silica," *Chemical Engineering Journal*, vol. 153, pp. 70–79, 2009. doi:10.1016/j.cej.2009.06.016.

[4] U. Wingenfelder, B. Nowack, G. Furrer, and R. Schulin, "Adsorption of Pb and Cd by amine-modified zeolite," *Water Research*, vol. 39, pp. 3287–3297, 2005. doi:10.1016/j.watres.2005.05.017.

[5] M. Cruz-Guzmán, R. Celis, M. C. Hermosín, W. C. Koskinen, E. A. Nater, and J. Cornejo, "Heavy metal adsorption by montmorillonites modified with natural organic cations," *Soil Science Society of America Journal*, vol. 70, p. 215, 2006. doi:10.2136/sssaj2005.0131.

[6] N. G. Turan and O. Ozgonenel, "Study of montmorillonite clay for the removal of copper (II) by adsorption: Full factorial design approach and cascade forward neural network," *The Scientific World Journal*, vol. 2013, 2013. doi:10.1155/2013/342628.

[7] S. R. Ha and K. Y. Rhee, "Effect of surface-modification of clay using 3-aminopropyltriethoxysilane on the wear behavior of clay/epoxy nanocomposites," *Colloids and Surfaces A: Physicochemical and Engineering Aspects*, vol. 322, pp. 1–5, 2008. doi:10.1016/j.colsurfa.2008.03.007.

[8] B. S. Krishna, D. S. R. Murty, and B. S. Jai Prakash, "Surfactant-modified clay as adsorbent for chromate," *Applied Clay Science*, vol. 20, pp. 65–71, 2001. doi:10.1016/S0169-1317(01)00039-4.

[9] K. G. Bhattacharyya and S. Sen Gupta, "Kaolinite, montmorillonite, and their modified derivatives as adsorbents for removal of Cu(II) from aqueous solution," *Separation and Purification Technology*, vol. 50, pp. 388–397, 2006. doi:10.1016/j.seppur.2005.12.014.

[10] B. S. Krishna, N. Mahadevaiah, D. S. R. Murty, and B. S. J. Prakash, "Surfactant immobilized interlayer species bonded to montmorillonite as recyclable adsorbent for lead ions," *Journal of Colloid and Interface Science*, vol. 271, pp. 270–276, 2004. doi:10.1016/j.jcis.2003.12.002.

[11] M. G. A. Vieira, M. L. Gimenes, and M. G. C. Da Silva, "Modelling of the process of adsorption of nickel in bentonite clay," *Chemical Engineering Transactions*, vol. 17, pp. 421–426, 2009. doi:10.3303/CET0917071.

[12] B. Riegel, S. Blittersdorf, W. Kiefer, S. Hofacker, M. Müller, and G. Schottner, "Kinetic investigations of hydrolysis and condensation of the glycidoxypropyltrimethoxysilane/aminopropyltriethoxy-silane system by means of FT-Raman spectroscopy I," *Journal of Non-Crystalline Solids*, vol. 226, pp. 76–84, 1998. doi:10.1016/S0022-3093(97)00487-0.

[13] M.-C. Brochier Salon and M. N. Belgacem, "Hydrolysis-condensation kinetics of different silane coupling agents," *Phosphorus, Sulfur, and Silicon*, vol. 186, pp. 240–254, 2011. doi:10.1080/10426507.2010.494644.

[14] P. Hesemann, T. Nguyen, and S. Hankari, "Precursor mediated synthesis of nanostructured silicas: from precursor-surfactant ion pairs to structured materials," *Materials*, vol. 7, pp. 2978–3001, 2014. doi:10.3390/ma7042978.

[15] P. C. Lebaron, Z. Wang, and T. J. Pinnavaia, "Polymer-layered silicate nanocomposites: An overview," *Applied Clay Science*, vol. 15, pp. 11–29, 1999. doi:10.1016/S0169-1317(99)00017-4.

[16] L. Liao, G. Lv, D. Cai, and L. Wu, "The sequential intercalation of three types of surfactants into sodium montmorillonite," *Applied Clay Science*, vol. 119, pp. 82–86, 2016. doi:10.1016/j.clay.2015.08.003.
[17] W. Luo, K. Sasaki, and T. Hirajima, "Surfactant-modified montmorillonite by benzyloctadecyldimethylammonium chloride for removal of perchlorate," *Colloids and Surfaces A: Physicochemical and Engineering Aspects*, vol. 481, pp. 616–625, 2015. doi:10.1016/j.colsurfa.2015.06.025.
[18] W. Luo, K. Sasaki, and T. Hirajima, "Effect of surfactant molecular structure on perchlorate removal by various organo-montmorillonites," *Applied Clay Science*, vol. 114, pp. 212–220, 2015. doi:10.1016/j.clay.2015.06.003.
[19] H. Senoussi, H. Osmani, C. Courtois, and H. Bourahli, "Mineralogical and chemical characterization of DD3 kaolin from the east of Algeria," *Boletín de la Sociedad Española de Cerámica y Vidrio*, vol. 55, no. 3, pp. 121–126, 2015.
[20] M. A. Zenasni, S. Benfarhi, A. Merlin, S. Molina, B. George, and B. Meroufel, "Adsorption of nickel in aqueous solution onto natural maghnite," *Mater Sci Appl.*, vol. 4, pp. 153–161, 2013. doi:10.4236/msa.2013.42018.
[21] F. Ayari, E. Srasra, and M. Trabelsi-Ayadi, "Removal of lead, zinc and nickel using sodium bentonite activated clay," *Asian Journal of Chemistry*, vol. 19, pp. 3325–3339, 2007.
[22] S. Lazarevic, I. Jankovic-Castvan, B. Jokic, D. Janackovic, and R. Petrovic, "Sepiolite functionalized with N-[3-(trimethoxysilyl)propyl]-ethylenediamine triacetic acid trisodium salt. Part II: Sorption of Ni2+ from aqueous solutions," *Journal of the Serbian Chemical Society*, vol. 81, pp. 197–208, 2016. doi:10.2298/JSC150525086L.
[23] R. Zare-Dorabei, S. M. Ferdowsi, A. Barzin, and A. Tadjarodi, "Highly efficient simultaneous ultrasonic-assisted adsorption of Pb(II), Cd(II), Ni(II) and Cu (II) ions from aqueous solutions by graphene oxide modified with 2,2'-dipyridylamine: Central composite design optimization," *Ultrasonics Sonochemistry*, vol. 32, pp. 265–276, 2016. doi:10.1016/j.ultsonch.2016.03.020.
[24] I. Mobasherpour, E. Salahi, and M. Pazouki, "Removal of nickel (II) from aqueous solutions by using nano-crystalline calcium hydroxyapatite," *Journal of Saudi Chemical Society*, vol. 15, pp. 105–112, 2011. doi:10.1016/j.jscs.2010.06.003
[25] M. Ghorbani, S. M. Nowee, N. Ramezanian, and F. Raji, "A new nanostructured material amino functionalized mesoporous silica synthesized via co-condensation method for Pb(II) and Ni(II) ion sorption from aqueous solution," *Hydrometallurgy*, vol. 161, pp. 117–126, 2016. doi:10.1016/j.hydromet.2016.02.002
[26] X. Zhang and X. Wang, "Adsorption and desorption of nickel(II) ions from aqueous solution by a lignocellulose/montmorillonite nanocomposite," *PLoS One*, vol. 10, no. 2, p. e0117077, 2015.
[27] M. R. Soares, J. C. Casagrande, and E. R. Mouta, "Nickel adsorption by variable charge soils: effect of pH and ionic strength," *Brazilian Archives of Biology and Technology*, vol. 54, no. 1, pp. 207-220, 2011.